scientific reports

Check for updates

OPEN

Complement C5 is not critical for the formation of sub-RPE deposits in *Efemp1* mutant mice

Donita L. Garland, Eric A. Pierce & Rosario Fernandez-Godino✉

The complement system plays a role in the formation of sub-retinal pigment epithelial (RPE) deposits in early stages of age-related macular degeneration (AMD). But the specific mechanisms that connect complement activation and deposit formation in AMD patients are unknown, which limits the development of efficient therapies to reduce or stop disease progression. We have previously demonstrated that C3 blockage prevents the formation of sub-RPE deposits in a mouse model of *EFEMP1*-associated macular degeneration. In this study, we have used double mutant *Efemp1*$^{R345W/R345W}$:*C5*$^{-/-}$ mice to investigate the role of C5 in the formation of sub-RPE deposits in vivo and in vitro. The data revealed that the genetic ablation of C5 does not eliminate the formation of sub-RPE deposits. Contrarily, the absence of C5 in RPE cultures promotes complement dysregulation that results in increased activation of C3, which likely contributes to deposit formation even in the absence of EFEMP1-R345W mutant protein. The results also suggest that genetic ablation of C5 alters the extracellular matrix turnover through an effect on matrix metalloproteinases in RPE cell cultures. These results confirm that C3 rather than C5 could be an effective therapeutic target to treat early AMD.

Age-related macular degeneration (AMD) is the most common cause of visual impairment in developed countries[1]. AMD begins as a progressive loss of fine central vision caused by degeneration of retinal pigment epithelial (RPE) cells and photoreceptors in the macular region[1]. While some therapies can delay the progression of AMD in patients at late stages (wet AMD), there is no cure for the most common form of disease (early/dry AMD), which affects millions of people worldwide[1]. The complex etiology of AMD and the absence of clinical biomarkers at early stages along with the diversity among patients, make it challenging to find effective therapeutic targets.

While AMD affects aged individuals, there are inherited maculopathies caused by mutations in single genes that manifest earlier in life, which makes them valuable tools to dissect the pathophysiology of AMD[2]. For instance, *EFEMP1*-associated macular degeneration, caused by the dominant mutation p.R345W in the EGF-containing fibulin-like extracellular matrix protein 1 (*EFEMP1*) gene shares clinical features with AMD, including the early appearance of sub-RPE deposits or drusen in the macula[3–6]. Drusen are deposits of protein and lipid that form between the basal lamina of the RPE and the connective tissue layer of the Bruch's membrane (BrM)[7,8]. Although the mechanisms for drusen formation and progression are not clear, it is known that the complement system, which is part of the immune system, plays an important role in drusen biogenesis[9,10].

The use of mouse models by our group and others has proved to be helpful for understanding the molecular mechanisms underlying the formation of sub-RPE deposits in macular degenerations, including insights about the role of the complement system in drusen formation[4–6,11–13]. For example, we have demonstrated that mice carrying the mutation p.R345W in *Efemp1* recapitulate the formation of basal deposits underneath the RPE, the composition of which is similar to those deposits observed in patients with this mutation and in AMD patients, including increased expression of C3 in the RPE/BrM interface[4,5]. Next, we showed that the blockage of complement activation mediated by the genetic ablation of *C3* had a protective effect, demonstrated by the absence of deposits in *Efemp1*$^{R345W/R345W}$:*C3*$^{-/-}$ mice[5]. The results were recapitulated by additional in vitro studies using primary RPE cells from mutant mice and human ARPE19-*EFEMP1*$^{R345W/R345W}$ cells[5,6,14]. In addition, the mutation p.R345W in *Efemp1* resulted in decreased matrix metalloproteinase (MMP) activity, which leads to altered extracellular matrix (ECM) turnover by *Efemp1*$^{R345W/R345W}$ RPE cells[6,15]. Such alterations are typically observed in drusen of AMD patients as well[16]. Overall, our previous data along with observations from other labs have proven that cell-based approaches can be also used to model some aspects of AMD[6,14,17,18].

Ocular Genomics Institute at Massachusetts Eye and Ear, Harvard Medical School, Boston, USA. ✉email: rosario_godino@meei.harvard.edu

The complement system can be activated by three different pathways (classical, lectin, and alternative), and C3 plays a central role in all of them, so the genetic ablation of *C3* inhibits the activation of the complement system by any pathway[19]. Activated C3b is required for the formation of the C5-convertase that, in turn, cleaves C5, leading to the generation of C5b and C5a and the assembly of the terminal membrane attack complex (MAC)[20,21]. Hence the absence of C3 prevents activation of C5 as well. A role for C5 in wet AMD has been demonstrated using mouse models[13,22,23] and some authors support the hypothesis that MAC plays a role in AMD pathogenesis, and that blocking C5 will have a protective effect for AMD patients[24]. Although the blockage of C5 did not show encouraging results in previous clinical trials (NCT00935883)[25], a recent trial using an aptamer anti-C5 has shown activity to reduce geographic atrophy[26]. Specific inhibition of C5 would prevent the generation of C5a and MAC, however, it would not prevent the complement functions associated with C3, such as immune clearance and opsonization. Indeed, the excess of C3b subunits available in a C5-depleted context would result in the formation of more C3-convertase, therefore, additional C3 activation[27,28]. Based on our previous research, we hypothesize that downregulation of C3 rather than C5 is required for preventing the formation of basal deposits in early stages of macular degenerations[5,6,14,17]. To address this question, in the current study we assessed the role of C5 in the formation of sub-RPE deposits in a mouse model of the *EFEMP1*-associated macular degeneration in vivo and in vitro. Our results show that knocking out C5 is not sufficient to prevent the formation of sub-RPE deposits in *Efemp1*$^{R345W/R345W}$ mice.

Results

Efemp1$^{R345W/R345W}$: C5$^{-/-}$ mice display sub-RPE deposits. Our group had previously shown a critical role for C3 in the formation of basal deposits by *Efemp1*$^{R345W/R345W}$ mice, demonstrated by the absence of deposits in double mutant *Efemp1*$^{R345W/R345W}$:*C3*$^{-/-}$mice and primary RPE cells[5,6]. The genetic ablation of C3 also inhibits the formation of the C5-convertase and further activation of C5 and MAC, which are known to play a role in wet AMD[22,23]. Thus, we first investigated if the inactivation of C5 was sufficient to prevent the formation of sub-RPE deposits.

Double mutant *Efemp1*$^{R345W/R345W}$:*C5*$^{-/-}$ mice were generated by crossing homozygous *Efemp1*$^{R345W/R345W}$ mice and homozygous *C5*$^{-/-}$ (B10.D2-Hc^{o} H2^{d} H2-T18^{c}/oSnJ) mice, which are serum C5 deficient[29]. The presence of sub-RPE basal deposits was determined in 14–18 month-old mice using transmission electron microscopy (TEM). As observed in our previous study, *Efemp1*$^{WT/WT}$:*C5*$^{+/+}$ mice exhibit normal basal infoldings in the RPE whereas the formation of extensive, sub-RPE basal deposits was observed in the *Efemp1*$^{R345W/R345W}$ mice (Fig. 1)[4,5]. As reported before[5], the basal infoldings of the RPE cells were lost and replaced by electrodense deposits. Low levels of small deposits have been observed with aging in wildtype and control mice as shown in Fig. 1 (Fig. 1b, c). Larger, more frequent basal deposits were present in the mutant *Efemp1*$^{R345W/R345W}$:*C5*$^{+/+}$ mice and double mutant *Efemp1*$^{R345W/R345W}$:*C5*$^{-/-}$ mice (Fig. 1d, e). The total area of basal deposits in the double mutant *Efemp1*$^{R345W/R345W}$:*C5*$^{-/-}$ mice trended slightly lower than in the *Efemp1*$^{R345W/R345W}$ mice, but the differences were not statistically significant (Fig. 1f). Thus, ablating C5 did not abolish the formation of basal deposits in *Efemp1*$^{R345W/R345W}$:*C5*$^{-/-}$ mice, indicating that C5 is not a good target to prevent the formation of sub-RPE deposits caused by the EFEMP1-R345W mutant protein.

Total area of basal deposits per length of the retinal slices from the temporal-ventral and nasal-dorsal quadrants at the level of the optic nerve were determined for the mutant and control mice (Fig. 1g). We observed that the extent of basal deposit formation varied between retinal quadrants with deposit formation, being typically maximal in the temporal-ventral quadrant (Fig. 1g). Although the morphology of basal laminar deposits was similar in both male and female mice, the amount, thickness, and continuity were greater in female mice (Fig. 1h).

Primary RPE cells from *Efemp1*$^{R345W/R345W}$: *C5*$^{-/-}$ mice recapitulate the formation of sub-RPE deposits in vitro. Primary RPE cells were isolated from 2 month old mice as previously described and were cultured on transwells to maintain the RPE properties in vitro[6,12]. Three days post seeding, the cells were present as a confluent monolayer of hexagonal bi-nucleated cells (Fig. 2a). Polarization of the RPE monolayer was demonstrated by transepithelial electrical resistance (TER) which reaches over 200 $\Omega \cdot cm^2$ by 72 h and remains stable for at least two weeks (Fig. 2b).

To further investigate the role of C5 in the formation of sub-RPE deposits in vitro, primary RPE cells from *Efemp1*$^{WT/WT}$:*C5*$^{+/+}$, *Efemp1*$^{R345W/R345W}$:*C5*$^{+/+}$, *Efemp1*$^{R345W/R345W}$:*C5*$^{-/-}$, and *Efemp1*$^{WT/WT}$:*C5*$^{-/-}$ mice were cultured on transwells for two weeks in the absence of serum. Analysis of flat mounts of the bottom side of the insert with scanning electron microscope (SM) showed that primary cells from *Efemp1*$^{R345W/R345W}$:*C5*$^{-/-}$ mice made sub-RPE deposits similar to those made by the *Efemp1*$^{R345W/R345W}$:*C5*$^{+/+}$ cells (Fig. 3), supporting that the absence of C5 is not protective against the formation of basal deposits. The size of basal deposits observed in old *Efemp1*$^{WT/WT}$:*C5*$^{-/-}$ mice trended slightly higher than wild type mice (Fig. 1f). Such feature was recapitulated in vitro, where RPE cells from *Efemp1*$^{WT/WT}$:*C5*$^{-/-}$ mice were observed to generate large sub-RPE deposits (Fig. 3). This finding suggests that the complement dysregulation observed in vivo associated with the absence of C5 is aggravated in RPE cultures, resulting in the formation of basal deposits even in the absence of the EFEMP1 mutant protein.

Based on our previous results using *Efemp1*$^{R345W/R345W}$ mice[5,6], we characterized the RPE cell cultures and basal deposits by immunostaining of vibratome sections and flat mounts of RPE cultured on transwells. As expected, we found increased expression of EFEMP1 in *Efemp1*$^{R345W/R345W}$:*C5*$^{+/+}$ and *Efemp1*$^{R345W/R345W}$:*C5*$^{-/-}$ cell cultures compared to controls (Fig. 4a)[6]. A strong immunostaining for C3 was observed in RPE cells carrying the *Efemp1*$^{R345W/R345W}$ allele compared to WT, especially in *Efemp1*$^{R345W/R345W}$:*C5*$^{-/-}$ cell cultures (Fig. 4a). Of note, the long-last staining with this antibody likely corresponds to the opsonins C3d and C3dg derived from the cleavage of C3, since C3b has a much shorter half-life[30]. To confirm the absence of C5 activation, we performed immunostaining with antibodies for MAC. The fluorescent confocal images did not show differential activation

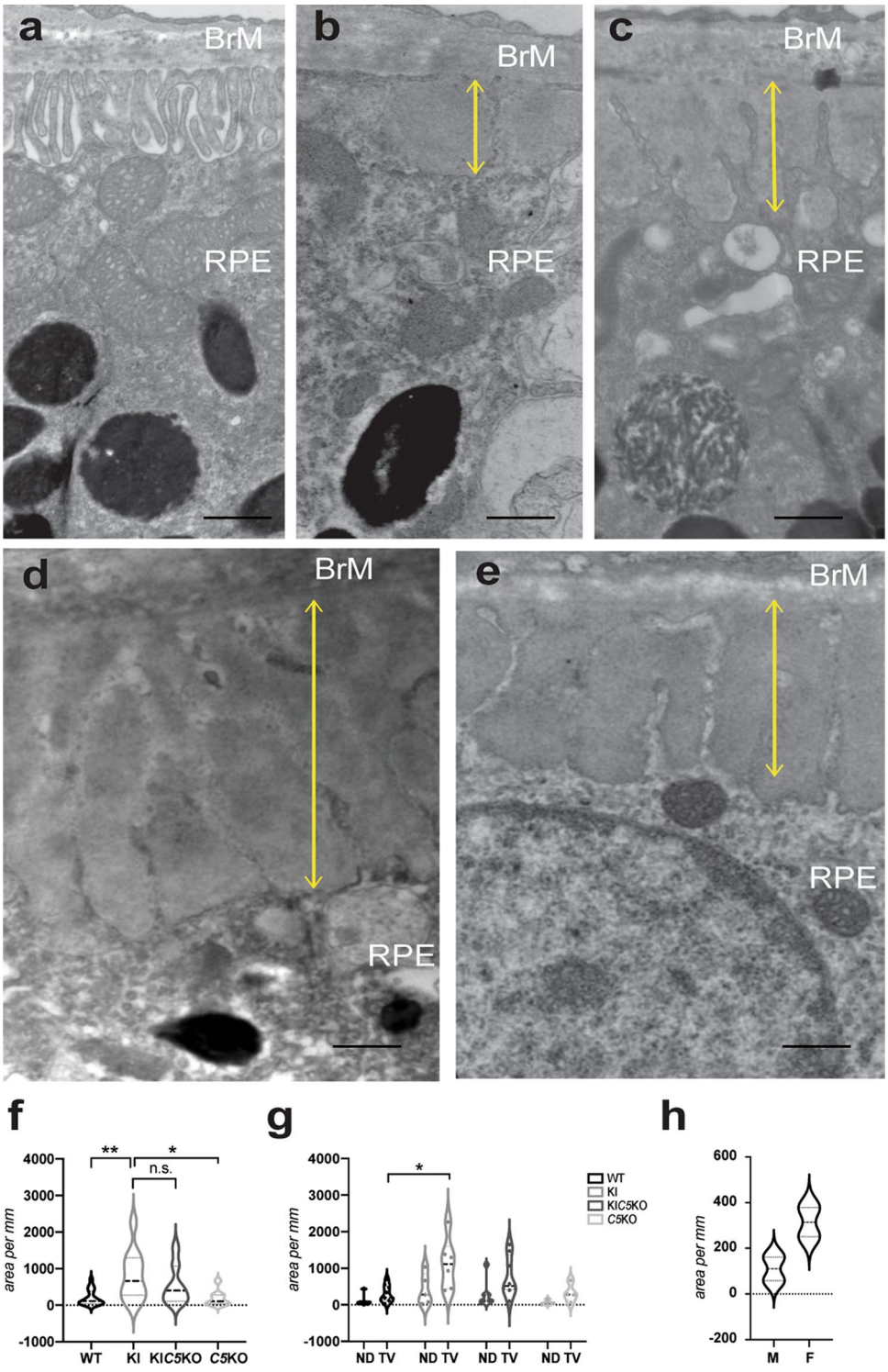

Figure 1. Transmission electron micrographs (TEM) of sub-RPE basal laminar deposits. (**a**) RPE with typical basal infoldings in *Efemp1*$^{WT/WT}$:*C5*$^{+/+}$ mice. With age, control mice may show some regions where basal infoldings are disrupted or missing and small sub-RPE deposits are observed: (**b**) *Efemp1*$^{WT/WT}$:*C5*$^{+/+}$ (**c**) and *Efemp1*$^{WT/WT}$:*C5*$^{-/-}$. (**d**) Larger, more frequent sub-RPE deposits are observed in *Efemp1*$^{R345W/R345W}$, and (**e**) *Efemp1*$^{R345W/R345W}$:*C5*$^{-/-}$ mice of the same age. Yellow lines mark the depth of the basal deposits. Scale bar = 500 nm. (**f–g**) Graphic representation of sub-RPE deposits measured as deposit area per mm length of retinal sections analyzed by TEM (average ± SD) in mice of all genotypes at 14–18 months of age. ND: nasal-dorsal, TV: temporal-ventral. (**h**) Violin plots represent the quantification of sub-RPE deposits in male vs. female *Efemp1*$^{R345W/R345W}$ mice at 12 months as deposit area per mm of retinal section analyzed by TEM. Note that the means of cumulative areas for the deposits at 14–18 months (**f–g**) are substantially larger than at 12 months (**g**). This growth rate has been reported before. F: female, M: male. Statistical analysis by 2-way ANOVA. **p < 0.01, *p < 0.05, n.s. = non-significant. N = 9 *Efemp1*$^{WT/WT}$:*C5*$^{+/+}$ (WT), n = 6 *Efemp1*$^{R345W/R345W}$:*C5*$^{+/+}$ (KI), n = 8 *Efemp1*$^{R345W/R345W}$:*C5*$^{-/-}$ (KIC5KO), n = 4 *Efemp1*$^{WT/WT}$:*C5*$^{-/-}$ (C5KO).

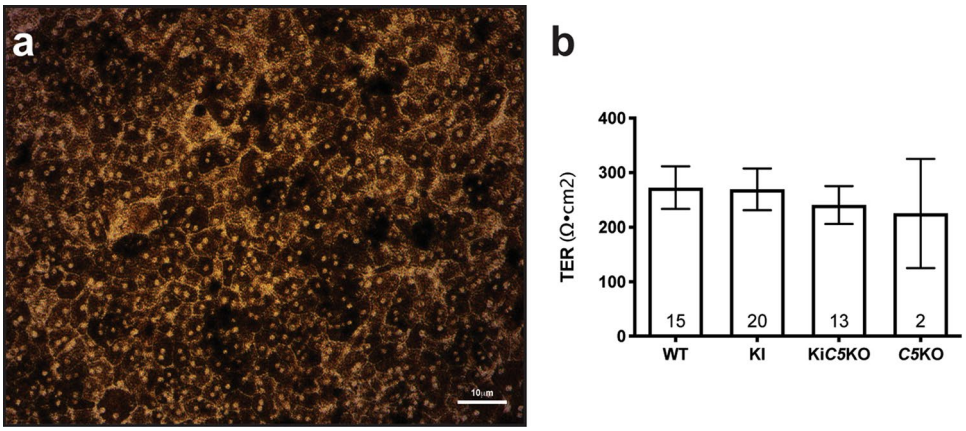

Figure 2. (**a**) Brightfield micrograph of mouse RPE cells *Efemp1*$^{R345W/R345W}$:*C5*$^{-/-}$ after two weeks on transwells confirms the formation of a healthy pigmented monolayer with honeycomb morphology. (**b**) Transepithelial electrical resistance (TER) measured after two weeks is similar in all cell cultures regardless the genotype.

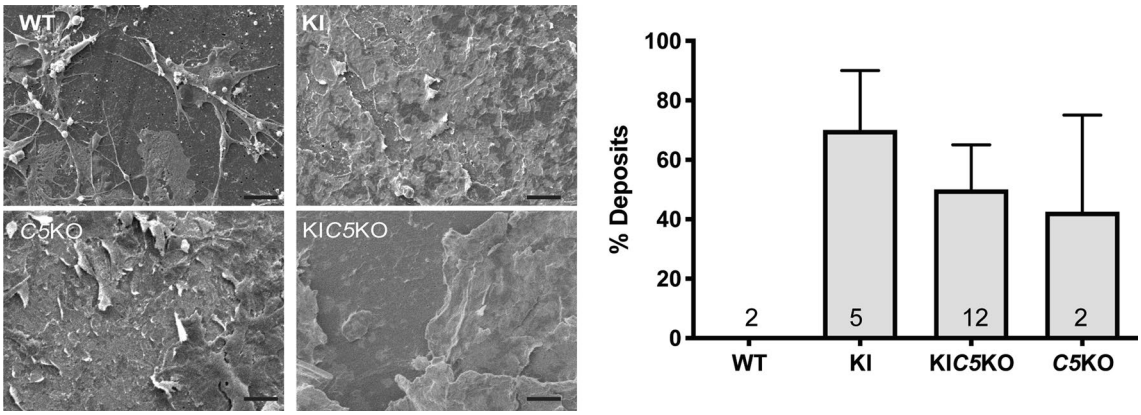

Figure 3. SM images of flat mounts of the bottom side of the transwell show filopodia that extend from the upper side through the pores of the insert in the *Efemp1*$^{WT/WT}$:*C5*$^{+/+}$ cultures (WT), vs. deposition of extracellular material in *Efemp1*$^{R345W/R345W}$:*C5*$^{+/+}$ (KI), *Efemp1*$^{R345W/R345W}$:*C5*$^{-/-}$ (KIC5KO) and *Efemp1*$^{WT/WT}$:*C5*$^{-/-}$ (*C5*KO) cultures**.** The graph represents the percentage of deposits measured in SM images using a pinpoint technique (see methods section). Data represented as average ± SEM, the numbers inside the bars indicate the amount of cultures used for quantification for each genotype. Scale bar = 10 µm. N = 2 *Efemp1*$^{WT/WT}$:*C5*$^{+/+}$ (WT), n = 5 *Efemp1*$^{R345W/R345W}$:*C5*$^{+/+}$ (KI), n = 12 *Efemp1*$^{R345W/R345W}$:*C5*$^{-/-}$ (KIC5KO), n = 2 *Efemp1*$^{WT/WT}$:*C5*$^{-/-}$ (C5KO).

of MAC in *Efemp1*$^{R345W/R345W}$:*C5*$^{+/+}$ mutant cells compared to *Efemp1*$^{WT/WT}$:*C5*$^{+/+}$ (Fig. 4a). As expected, we did not detect MAC in *C5*$^{-/-}$ cells (Fig. 4a).

To characterize the composition of the sub-RPE deposits made by primary cells in vitro, flat mounts of the bottom side of the inserts containing RPE cells were immunostained with antibodies for the ECM proteins that typically accumulate in basal deposits of AMD patients[31]. As previously reported for *Efemp1*$^{R345W/R345W}$ mutant mice and RPE cultures, we detected accumulation of elastin, TIMP3 and EFEMP1 secreted by the RPE to the bottom side of the insert in *Efemp1*$^{R345W/R345W}$:*C5*$^{-/-}$ cultures (Fig. 4b)[31]. This could be due to a differential role of mutant EFEMP1 in elastogenesis[32] or higher affinity to bind TIMP-3[33]. In this study, EFEMP1 was homogeneously deposited along the insert, and accumulated in *Efemp1*$^{R345W/R345W}$:*C5*$^{+/+}$ and *Efemp1*$^{R345W/R345W}$:*C5*$^{-/-}$ cultures compared to wildtype. Excessive deposition of CFH associated with the presence of EFEMP1-R345W mutant protein was also observed in *Efemp1*$^{R345W/R345W}$:*C5*$^{+/+}$ and *Efemp1*$^{R345W/R345W}$:*C5*$^{-/-}$ cultures (Fig. 4b). Of note, EFEMP1 and CFH co-localized on the deposits (Fig. 4b), which confirms the interaction of these two proteins in the ECM[34].

RPE cells from *Efemp1*$^{R345W/R345W}$: *C5*$^{-/-}$ mice secrete increased amounts of C3. We have previously demonstrated that C3 is necessary for the formation of basal deposits in mice and RPE cells with the p.R345W mutation in *Efemp1*[5,6]. Our previous experiments using primary mouse RPE cells showed that *Efemp1*$^{R345W/R345W}$ cells secreted increased amounts of C3[6]. In the current studies, we measured the amount of C3 secreted to the conditioned media by wildtype and mutant cells via ELISA. In concordance with the strong C3 immunostaining observed in the vibratome sections, elevated levels of C3 detected in conditioned media from *Efemp1*$^{R345W/R345W}$: *C5*$^{+/+}$ cultures (2-way ANOVA, p = 0.0195) (Fig. 5). In the absence of C5, the levels of C3

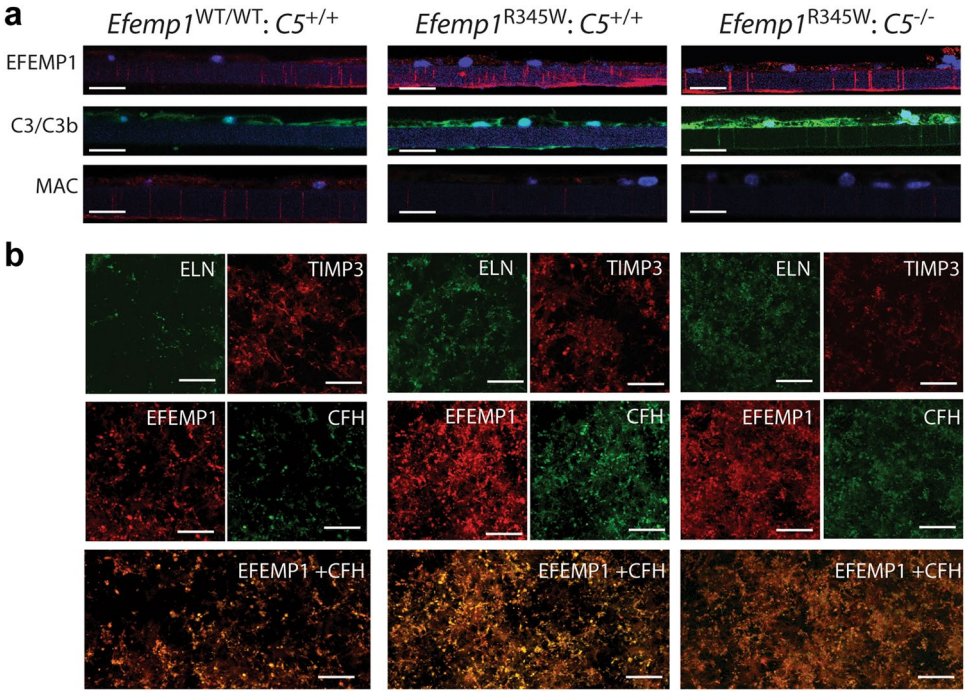

Figure 4. (**a**) Vibratome sections of primary mouse RPE cells *Efemp1*$^{WT/WT}$:*C5*$^{+/+}$, *Efemp1*$^{R345W/R345W}$:*C5*$^{+/+}$, and *Efemp1*$^{R345W/R345W}$:*C5*$^{-/-}$ cultured on transwells for two weeks and immunostained with antibodies for EFEMP1, C3/C3b/iC3b/C3d and C3dg, MAC. Note positive C3 staining at the bottom of the insert in *Efemp1*$^{R345W/R345W}$:*C5*$^{+/+}$ cultures and throughout the insert pores in *Efemp1*$^{R345W/R345W}$:*C5*$^{-/-}$ cultures. This is due to the orientation of the sections. (**b**) Flat mounts of the bottom side of the inserts were immunostained with antibodies for ELN, TIMP-3, EFEMP1, CFH. EFEMP1 and CFH colocalize in the deposits. Scale bars a-i: 25 µm, j-aa: 100 µm.

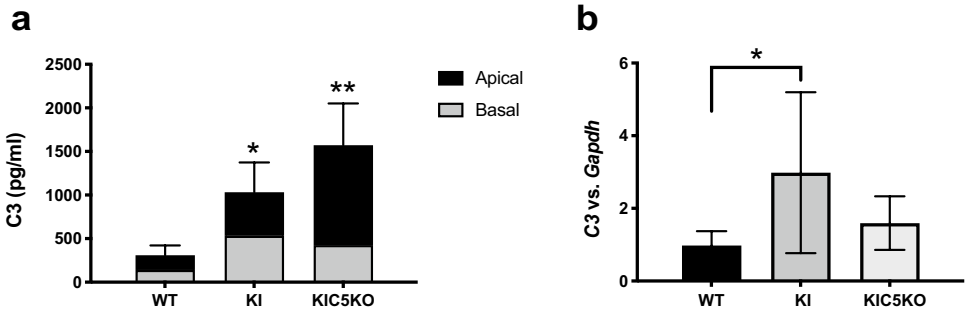

Figure 5. Levels of C3 measured by ELISA in the apical and basal conditioned media of RPE cultures showed increased levels of C3 in *Efemp1*$^{R345W/R345W}$:*C5*$^{+/+}$ and *Efemp1*$^{R345W/R345W}$:*C5*$^{-/-}$ cultures compared to controls. Data from apical and basal side were combined for statistics. This represents the reality with better accuracy, since the basal conditioned media needs to be concentrated three times more, which results in more protein lost in the Amicon filter. Also C3 proteins secreted to the basal side can remain trapped inside the pores of the transwells[18]. Data represented as average ± SD (2-way ANOVA, $^{*}p < 0.05$, $^{**}p < 0.01$).

detected in conditioned media from *Efemp1*$^{R345W/R345W}$: *C5*$^{-/-}$ cells increased an additional 50% (2-way ANOVA, $p = 0.0035$). Although the ELISA utilized can detect intact C3 as well as cleaved C3, based on the immunostaining results, the higher levels of C3 detected by ELISA are likely due to its increased activation.

Depletion of C5 restores MMP-2 activity in mutant *Efemp1*$^{R345W/R345W}$ RPE cells. We have previously reported that MMP-2 activity diminishes in conditioned media of mouse *Efemp1*$^{R345W/R345W}$ RPE cells, and it does not change in the presence or absence of C3[6]. To assess whether the absence of C5 had an impact on the ECM turnover, we used zymography analyses, which allows measurement of the collagenase activity of MMP-2, which is secreted by the RPE and mediates the ECM turnover of the BrM[35]. The collagenase activity detected in conditioned media of *Efemp1*$^{R345W/R345W}$: *C5*$^{-/-}$ cells was similar to the activity found in wildtype controls, which slightly differs from the MMP-2 activity found in *Efemp1*$^{R345W/R345W}$: *C5*$^{+/+}$ and *Efemp1*$^{R345W/R345W}$: *C3*$^{-/-}$ cells

(Supplementary Fig. 1). Although differences are not statistically significant, the absence of C5 attenuates the loss of MMP-2 activity associated with the EFEMP1 mutant protein.

Discussion

Genetic and clinical studies have demonstrated a role for the complement system in the formation of drusen in early stages of AMD, but defining the extent to which each complement component contributes to this disease is critical for the identification of efficient therapeutic targets[31,36–42]. To address this need, in this study we have used mouse and cell-based models of macular degeneration to investigate the role of C5 in the formation of sub-RPE deposits[4–6,17]. The in vivo and in vitro studies showed that the genetic ablation of C5 is not sufficient to prevent the formation of basal deposits underneath the RPE in a mouse model of the inherited *EFEMP1*-associated macular degeneration. Indeed, the ablation of C5 enhances the accumulation of basal deposits underneath the RPE in vitro even in the absence of the EFEMP1-R345W mutant protein. In addition, blockage of C5 enhances the activation of the complement system mediated by increased amounts of C3 secreted by the RPE in culture. Consistent with previous studies in our lab, the increased levels of C3 observed in *Efemp1*$^{R345W/R345W}$: *C5*$^{-/-}$ cell cultures point at C3 as a major contributor for basal deposit formation[5,6,14,17]. These results could explain the failure of C5-targeted treatments in clinical trials and supports the potential of C3 as a therapeutic target to reduce drusen progression.

In the absence of complement C5, the number and size of basal laminar deposits in *Efemp1*$^{R345W/R345W}$ mice were diminished but not eliminated. This is in contrast to previously reported results that demonstrated that genetic ablation of C3 prevented the formation of basal laminar deposits due to the EFEMP1-R345W mutant protein[5,6]. Therefore, inhibition of C5 is not protective against deposit formation. Indeed, the absence of C5 is sufficient to propel accumulation of material underneath the RPE in vitro, likely associated with the positive feedback loop that increases C3[28]. This dysregulation of the complement system caused by a long-term C5 inhibition is typically observed in patients with glomerular disease, who develop C3-associated deposits in the kidney comparable to those developed by patients with deficiencies in CFH and CFI[28,43]. Our in vitro model offers a pure environment without external complement regulators normally found in serum and tissues. Unlike plasma, where CFH accelerates its inactivation, C3 in cell culture media could participate in the assembly of more convertase, generating the positive feedback loop measured as increased levels of C3 in RPE cells and conditioned media of *Efemp1*$^{R345W/R345W}$: *C5*$^{-/-}$ cultures[21,27].

As we reported previously, the sub-RPE deposits found in primary cultures of both *Efemp1*$^{R345W/R345W}$: *C5*$^{+/+}$ and *Efemp1*$^{R345W/R345W}$: *C5*$^{-/-}$ mice are comprised of excessive depositions of normal ECM proteins[6,14]. Positive immunostaining with antibodies for EFEMP1, TIMP-3 and elastin, confirmed that the deposits made by RPE cells *Efemp1*$^{R345W/R345W}$: *C5*$^{+/+}$ and *Efemp1*$^{R345W/R345W}$: *C5*$^{-/-}$ are similar in composition to basal laminar deposits and drusen found in AMD patients[31]. Intensified immunostaining of elastin may indicate a differential role of mutant EFEMP1 in elastogenesis[32]. The immunostaining also revealed an intensified deposition of CFH underneath the RPE in the presence of the EFEMP1-R345W mutant protein. This phenomenon can be explained by the fact that EFEMP1 binds CFH[34]. Wyatt and collaborators demonstrated a higher affinity of the AMD-risk associated variant CFH-402H for EFEMP1 compared to the low-risk allele CFH-402Y[34]. Given that the mutation p.R345W is located in the protein domain where EFEMP1 binds CFH, it is possible that mutant EFEMP1-R345W has higher affinity for CFH than EFEMP1-WT, which would favor the inclusion of CFH in the protein aggregates typically originated by EFEMP1-R345W[6]. CFH sequestered into protein aggregates will likely lose its complement regulatory function, which contributes to the increased levels of C3 found in these cultures. This process shares features with the impaired complement regulation in the BrM with age, associated with the loss of heparan sulfate proteoglycan, which is responsible for anchoring CFH to the BrM, and that is exacerbated in the context of the AMD risk allele *CFH*-Y402H[44].

For the first time, we have characterized the regional localization of sub-RPE deposits in *Efemp1*$^{R345W/R345W}$ mice, which are more abundant in the temporal-ventral quadrant. This finding could be explained by the higher RPE cell density, including more bi-nucleated cells, present in the ventral-central region of mice retinas[45]. Likewise, in humans, RPE cell density is highest in the central temporal retina[46], where the macula is located, and where the rate of apoptosis increases with age[47]. Higher levels of deposit formation were observed in female mice, which could be explained by a deficiency of estrogen described in older female rodents[48]. In humans, the beneficial effect of estrogens for the retina has been demonstrated by a higher risk of AMD in women who enter menopause at young age[49]. In mice, age-related estrogen deficiency increases susceptibility to sub-RPE deposition caused by dysregulating turnover of BrM, which contributes to thickening of collagenous layers[50]. Other studies in our lab have demonstrated a key role for the BrM turnover in the formation of sub-RPE deposits[6,14,15]. Also, estrogen can regulate signaling pathways involved in AMD pathogenesis through its anti-oxidative and anti-inflammatory effect[51]. Indeed, gender specific effects on autoimmune disorders and on immune cell populations are beginning to be appreciated[52]. Further studies should be performed to determine the protective role of estrogens in the retina.

Based on our previous studies, we expected the MMP-2 activity to be diminished in the conditioned media of *Efemp1*$^{R345W/R345W}$ RPE cells[6], however, in the absence of C5, the MMP-2 activity was restored to normal levels, which would reinstate the normal ECM turnover. We and others have demonstrated that C3a can modulate the activity of MMP-2[6,17,53]. Thereby, the increased MMP-2 activity observed in the *Efemp1*$^{R345W/R345W}$:C5$^{-/-}$ cultures could be a secondary effect driven by overactivation of C3. Nonetheless, abnormal ECM deposition is observed in *Efemp1*$^{R345W/R345W}$:C5$^{-/-}$ cultures, which suggests that fine regulation of the ECM turnover is not sufficient to restore the homeostasis in the RPE *Efemp1*$^{R345W/R345W}$:C5$^{-/-}$ cells.

Based on this and other studies in our lab, we believe that the increased activation of C3 in *Efemp1*$^{R345W/R345W}$ cells occurs via tick-over, through deposition of C3b on the EFEMP1-derived abnormal ECM, which prevents its

futile depletion and enhances the stabilization of the tick-over convertase on the substrate[6,14,54]. This hypothesis is sustained by the positive immunostaining for C3b in the abnormal ECM secreted by mutant *Efemp1*$^{R345W/R345W}$ RPE cells. Of note, C3b deposited on the ECM that is not inactivated by CFH will result in chronic activation of C3 by the mediated by the canonical C3-convertase of the alternative pathway, which is also dysregulated in the absence of C5[21,54,55]. Another possibility is that mutant EFEMP1 causes presentation of ligands that lead to the activation of the classical pathway. In any case, complement activity would be mediated by C3, but does not require the activation of C5 or MAC. Further analyses would be required to define whether the activation of C3 occurs via tick-over or the canonical pathway.

In conclusion, blockage of C5 is not sufficient to protect against the formation of sub-RPE deposits, which may explain the inefficiency of some anti-C5 therapies in the clinic[25,56]. While phase II trials using a PEGylated anti-C5 aptamer have shown efficiency to reduce geographic atrophy[26], the inhibition of C5 may not be applicable to prevent disease progression at early-stage AMD. Instead, C3 inhibitors are expected to provide a broader therapeutic coverage. While their activity to reduce geographic atrophy has been strongly supported by phase II trials (FILLY trial), previous studies have also confirmed their efficiency to reduce basal deposit formation[5,17]. Thereby, therapeutic strategies to prevent C3 rather than C5 activation may prove to be more successful to treat patients with early-intermediate stage AMD.

Methods

Mice. All the experiments were approved by the Mass Eye and Ear Animal Care and Use Committee and followed the guidelines of the ARVO Statement for the Use of Animals in Ophthalmic and Vision Research. This study was performed in compliance with the ARRIVE guidelines.

The *Efemp1*$^{R345W/R345W}$ mice, made and characterized previously, were generated from het x het crossings[4]. Wildtype littermates generated during het x het crosses of *Efemp1*$^{WT/R345W}$ mice were used as controls. *Efemp1*$^{R345W/R345W}$ mice were crossed with homozygous C5$^{-/-}$ mice (B10.D2-Hc^{0} H2^{d} H2-T18^{c}/o2SnJ) purchased from Jackson Laboratory (JAX stock #000,461), which have a 2 base deletion that creates a STOP codon and results in a non-functional protein. None of these mice contained the *rd8* mutation[57]. Mice were genotyped for the *Efemp1* mutation as previously described[5]. Briefly, DNA was extracted from mouse tails using the Allele-In-One Mouse Tail Direct Lysis Buffer (Allele Biotechnology) following manufacturer's instructions. For the C5 genotype, DNA was amplified by PCR using the following primers: forward 5' TTGCTTCCACAGGTATGGTG 3' and reverse 5' CCCCACCCTCTTCTGGTACT 3'. Two µl of DNA (30–50 ng) were mixed with 0.4 µM of each primer, 1.5 mM of $MgCl_2$, 0.2 mM of dNTPs, 1X of buffer 2, 1X of solution S and 0.5 units of HotFire Taq (Solis Biodyne) in a final volume of 25 µl. The mix was amplified in a thermal cycler using the following program: 95° for 15 min, followed by 35 cycles of 95° for 1 min, 52° for 1 min, and 72° for 1 min. Final extension step was 72° for 5 min. The PCR product was then sequenced by Sanger using the forward primer to detect the 2 bp deletion[58].

Transmission electron microscopy (TEM). 14–18-month-old mice were euthanized by CO_2 asphyxiation and immediately perfused with 4% paraformaldehyde[5]. Eye orientation was marked with a fine cautery tip before enucleation. The enucleated eye globes were promptly placed in half strength Karnovsky's fixative (2% formaldehyde + 2.5% glutaraldehyde, in 0.1 M sodium cacodylate buffer, pH 7.4) and fixed for 4 h. Next, the cornea and lens were removed by cutting around the *ora serrata*. The eye cups were kept in fresh fixative overnight at 4° C, rinsed with 0.1 M sodium cacodylate buffer three times and stored at 4° C until they were embedded. Subsequent steps, including post-fixation, *en bloc* staining, embedding, sectioning of the blocks and imaging were all performed in the Schepens/MEE Morphology Core. Briefly, samples were post-fixed with 2% osmium tetroxide in 0.1 M sodium cacodylate buffer for 1.5 h, *en bloc* stained with 2% aqueous uranyl acetate for 30 min and dehydrated with graded ethyl alcohol solutions. The samples were resin infiltrated in ethyl alcohol and Spurr's resin epoxy mixtures using an automated EMS Lynx 1 EM tissue processor (Electron Microscopy Sciences). Processed samples were infiltrated with two changes of fresh Spurr's resin for 24 h and the samples were then oriented in the resin. The resin was polymerized within silicone molds using an oven at 60 °C for a minimum of 24 h. The samples were en bloc stained with 2% uranyl acetate for 30 min. Semi-thin sections for light microscopy were cut in cross-section at 1-micron and stained with 1% toluidine blue in 1% sodium tetraborate aqueous solution for assessment and screening regions of the processed samples for thin sectioning. Ultrathin Sects. (70 nm) were cut using a diamond knife and were collected onto single slot formvar-carbon coated grids. The retinal sections were cut at the level of the optic nerve and extended from the optic nerve outwards to the ora serrate in the temporal/ventral quadrant and in the dorsal/nasal quadrant. The sections were not post stained. The grids were imaged at a direct magnification of 18,500 using a FEI Tecnai G2 Spirit transmission electron microscope at 80 kV. The microscope was interfaced with an AMT XR41 digital CCD camera for digital TIFF file image acquisition.

To systematically assess basal laminar deposit formation, images were acquired of all basal deposits along the entire length of each thin section at a direct magnification of 18,500. Both the temporal/ventral and dorsal/nasal quadrants at the level of the optic nerve were analyzed since deposit formation was not equivalent within the 4 retinal quadrants. The areas of the deposits were determined by manually outlining the deposits in each image and determining the areas using ImageJ. If the images were not acquired at a direct magnification of 18,500 the results were normalized to that magnification. The areas of all deposits were summed for the sections from the two quadrants per mouse and reported as area (μ^2/mm). Deposits were present in the peripapillary region of the sections of most eyes. The areas of these deposits were excluded from the analyses because they were associated with incompletely formed or degrading RPE cells. For all samples in which the deposits in these areas were measured, the areas were similar in each eye. A minimum of 65 micrographs were taken per mouse.

Mouse RPE cell isolation. RPE cells were harvested from 10-week-old mice following CO2-induced euthanasia. Eyes were dissected and RPE cells were collected by enzymatic digestion as previously described[6,12]. Briefly, eyecups were dissected and the neural retina was separated from the RPE with 1 mg/ml of hyaluronidase. The RPE cells were detached from the BrM with trypsin and collected in RPE media with 20% FBS. Isolated cells were resuspended in RPE media containing 5% of FBS and seeded on 6.5 mm transwells coated with laminin following published methods[6,12].

RPE cell cultures. Cells were cultured at 37 °C in 5% CO2 under a humidified atmosphere changing media twice a week. Serum was removed 72 h post seeding on transwells. Transepithelial electrical resistance (TER) of the RPE cultures were measured using an epithelial voltohmmeter (EVOM)[59].

RNA extraction and quantitative real time (qRT)-PCR. was performed as previously described[6]. RNA was extracted from RPE cultures after 2 weeks on transwells using the DNA/RNA/Protein Mini Kit (Qiagen). The amount of RNA and its integrity were measured with the Agilent RNA 6000 Nano Kit Bioanalyzer (Agilent Technologies). Only samples with RIN values between 9 and 10 were used for cDNA synthesis with the Affinity Script cDNA Synthesis kit (Agilent Technologies). Briefly, 5 ng of cDNA, 200 nM of each primer and 10 µl of Fast SYBR Green were combined. Amplification was done in the Stratagene Mx3000P® QPCR system using the following program: 95 °C for 20 s, 40 cycles of 95 °C for 3 s, 60 °C for 30 s followed by melting curve. Each sample was assayed in triplicate. *Gapdh* was used as an endogenous control and the wildtype sample was set to a value of 1 to be used as a calibrator. Primers used for amplification are the following: *C3* (forward 5'-TCC TGAACTGGTCAACATGG-3' and reverse 5'-AAACTGGGCAGCACGTATTC-3').

ELISA. Apical and basal conditioned media from RPE cell cultures were collected after 2 weeks in culture and concentrated to equal volumes through 10 kDa Amicon filters (Millipore, Billerica, MA). The fraction over 10 kDa was used to quantify C3 using the ALPCO ELISA kit.

Characterization of Deposits in vitro. Deposits were characterized by SM and immunofluorescence as previously described[6].

Scanning electron microscopy. RPE cells grown on inserts were fixed in cold 4% PFA in PBS followed by fixation in 1% glutaraldehyde, washed in PBS and then in dH2O and dehydrated by serial ethanols, 35%, 50%, 70%, 95%, 95% and 100% followed by critical dehydration using the SAMDRI-795 system. After dehydration, inserts were split into 2 pieces and the top or bottom side was coated with chromium using a Gatan Ion Beam Coater for 10 min. Coated inserts were imaged by Field Emission Scanning Electron Microscope (JEOL 7401F).

Pinpoint technique to quantify basal deposits. The percentage of deposit formation was defined as the percentage of SM images positive for deposits divided by the total number of images taken of the whole insert (# images per equal parts insert). A minimum of 10 images was taken per sample. The experimenter was masked to the sample identity.

Vibratome sections. RPE cells on transwells were fixed for 10 min in cold 4% paraformaldehyde (PFA) in PBS followed by fixation in 1% glutaraldehyde for 30 min at RT. The insert was then removed and split with a razor blade into small fragments of 2.5 mm × 5 mm, which were embedded into 10% Agarose XI as previously published[12]. Sections of 100 µm were performed at medium speed (around 5) and amplitude (approx. 6) using a vibratome Leica VT1000S (Leica). Sections were placed on a glass slide for immunostaining.

Immunostaining. Cell inserts were rinsed in PBS, fixed for 10 min in cold 4% PFA in PBS followed by fixation in 1% glutaraldehyde for 30 min at RT. The inserts were cut off with a razor blade and stored in PBS at 4 °C pending sectioning and immunohistochemical analyses. To analyze the bottom side of the inserts, they were placed face down on slides as flat mounts. For staining, slides containing flat mounts or vibratome sections were blocked with 1% BSA and incubated with primary antibodies anti C3/C3b/iC3b/C3d/C3dg (AB11862, Abcam), EFEMP1 (SDIX), MAC (C5b-9 AB55811, Abcam), TIMP-3 (AB39184 Abcam), ELN (sc17581, Santa Cruz Biotechnology), and CFH (AB53800, Abcam) overnight at 4 °C. Secondary antibodies labeled with Alexa-488 or Alexa-555 were incubated for 1 h at RT. Slides were mounted with Fluoromount G and visualized by TCS SP5 II confocal laser scanning microscope (Leica). Samples incubated with 1% BSA instead of primary antibody were used as negative controls.

MMP-2 activity. Was measured in conditioned media from RPE cultures by zymography as previously described[6]. Briefly, 5 µl of equal volume supernatants were loaded onto Novex 10% gelatin gels (Life Technologies). Zymography assays were then performed per manufacturer's instructions. Gels were scanned using the Odyssey system (Li-Cor). MMP-2 was identified by molecular weight. Gelatinase activity was quantified using densitometry and the software ImageStudioLite (Li-Cor).

Statistical analyses. Results are expressed as mean ± SD or SEM, with $p < 0.05$ considered statistically significant. Differences between groups were compared using the Student t-test or ANOVA as appropriate using GraphPad Prism software.

Received: 23 January 2021; Accepted: 5 May 2021
Published online: 17 May 2021

References

1. Miller, J. W. Age-related macular degeneration revisited - Piecing the puzzle: The LXIX edward jackson memorial lecture. *Am. J. Ophthalmol.* **155**, 1-35.e13 (2013).
2. Michaelides, M., Hunt, D. M. & Moore, A. T. The genetics of inherited macular dystrophies. *J. Med. Genet.* **40**, 641–650 (2003).
3. Stone, E. M. *et al.* A single EFEMP1 mutation associated with both Malattia Leventinese and Doyne honeycomb retinal dystrophy. *Nat. Genet.* **22**, 199–202 (1999).
4. Fu, L. *et al.* The R345W mutation in EFEMP1 is pathogenic and causes AMD-like deposits in mice. *Hum. Mol. Genet.* **16**, 2411–2422 (2007).
5. Garland, D. L. *et al.* Mouse genetics and proteomic analyses demonstrate a critical role for complement in a model of DHRD/ML, an inherited macular degeneration. *Hum. Mol. Genet.* **23**, 52–68 (2014).
6. Fernandez-Godino, R., Garland, D. L. & Pierce, E. A. A local complement response by RPE causes early-stage macular degeneration. *Hum. Mol. Genet.* **24**, 5555–5569 (2015).
7. Sarks, S. H., Arnold, J. J., Killingsworth, M. C. & Sarks, J. P. Early drusen formation in the normal and aging eye and their relation to age related maculopathy: a clinicopathological study. *Br. J. Ophthalmol.* **83**, 358–368 (1999).
8. Sarks, S. H. Drusen Patterns Predisposing To Geographic Atrophy of the Retinal Pigment Epithelium. *Aust. J. Opthalmology* **10**, 91–97 (1982).
9. Anderson, D. H. *et al.* The pivotal role of the complement system in aging and age-related macular degeneration: Hypothesis revisited. *Prog. Retin. Eye Res.* **29**, 95–112 (2010).
10. Anderson, D. H., Mullins, R. F., Hageman, G. S. & Johnson, L. V. A role for local inflammation in the formation of drusen in the aging eye. *Am. J. Ophthalmol.* **134**, 411–431 (2002).
11. Marmorstein, L. Y., McLaughlin, P. J., Peachey, N. S., Sasaki, T. & Marmorstein, A. D. Formation and progression of sub-retinal pigment epithelium deposits in Efemp1 mutation knock-in mice: A model for the early pathogenic course of macular degeneration. *Hum. Mol. Genet.* **16**, 2423–2432 (2007).
12. Fernandez-Godino, R., Garland, D. L. & Pierce, E. A. Isolation, culture and characterization of primary mouse RPE cells. *Nat. Protoc.* **11**, 1206–1218 (2016).
13. Toomey, C. B. *et al.* Effect of anti-C5a therapy in a murine model of early/ intermediate dry age-related macular degeneration. *Investig. Ophthalmol. Vis. Sci.* **59**, 662–673 (2018).
14. Fernandez-Godino, R., Bujakowska, K. M. & Pierce, E. A. Changes in extracellular matrix cause RPE cells to make basal deposits and activate the alternative complement pathway. *Hum. Mol. Genet.* **27**, 147–159 (2018).
15. Fernandez-Godino, R., Pierce, E. A. & Garland, D. L. Extracellular matrix alterations and deposit formation in AMD. *Adv. Exp. Med. Biol.* **854**, 53–58 (2016).
16. Leu, S. T. *et al.* Drusen are cold spots for proteolysis: Expression of matrix metalloproteinases and their tissue inhibitor proteins in age-related macular degeneration. *Exp. Eye Res.* **74**, 141–154 (2002).
17. Fernandez-Godino, R. & Pierce, E. A. C3a triggers formation of sub-retinal pigment epithelium deposits via the ubiquitin proteasome pathway. *Sci. Rep.* **8**, 1–14 (2018).
18. Johnson, L. V. *et al.* Cell culture model that mimics drusen formation and triggers complement activation associated with age-related macular degeneration. *Proc. Natl. Acad. Sci. U. S. A.* **108**, 18277–18282 (2011).
19. Ricklin, D., Hajishengallis, G., Yang, K. & Lambris, J. D. Complement: A key system for immune surveillance and homeostasis. *Nat. Immunol.* **11**, 785–797 (2010).
20. Atkinson, J. P. & Farries, T. Separation of self from non-self in the complement system. *Trends Immunol.* **8**, 212–215 (1987).
21. Rawal, N. & Pangburn, M. K. Formation of High-Affinity C5 Convertases of the Alternative Pathway of Complement. *J. Immunol.* **166**, 2635–2642 (2001).
22. Nozaki, M. *et al.* Drusen complement components C3a and C5a promote choroidal neovascularization. *Proc. Natl. Acad. Sci. U. S. A.* **103**, 2328–2333 (2006).
23. Cashman SM, Ramo K, Kumar-Singh R. A non membrane-targeted human soluble CD59 attenuates choroidal neovascularization in a model of age related macular degeneration. PLoS One. 2011 Apr 28;6(4):e19078. https://doi.org/10.1371/journal.pone.0019078
24. Johnson, L. V., Ozaki, S., Staples, M. K., Erickson, P. A. & Anderson, D. H. A potential role for immune complex pathogenesis in drusen formation. *Exp. Eye Res.* **70**, 441–449 (2000).
25. Yehoshua, Z. *et al.* Systemic complement inhibition with eculizumab for geographic atrophy in age-related macular degeneration: The COMPLETE study. *Ophthalmology* **121**, 693–701 (2014).
26. Jaffe, G. J. *et al.* C5 inhibitor avacincaptad pegol for geographic atrophy due to age-related macular degeneration: a randomized pivotal phase 2/3 trial. *Ophthalmology* **128**, 576–586 (2021).
27. Rawal, N. & Pangburn, M. K. C5 convertase of the alternative pathway of complement: Kinetic analysis of the free and surface-bound forms of the enzyme. *J. Biol. Chem.* **273**, 16828–16835 (1998).
28. Smith-Jackson, K. *et al.* Hyperfunctional complement C3 promotes C5-dependent atypical hemolytic uremic syndrome in mice. *J. Clin. Invest.* **129**, 1061–1075 (2019).
29. Wetsels, A., Fleischer, T. & Haviland, D. L. Deficiency of the murine fifth complement component (C5). *J. Biol. Chem.* **265**, 2435–2440 (1990).
30. Pangburn, M. K. & Muller-Eberhard, H. J. The C3 convertase of the alternative pathway of human complement Enzymic properties of the bimolecular proteinase. *Biochem. J.* **235**, 723–730 (1986).
31. Curcio, C. A. & Johnson, M. Structure, Function, and Pathology of Bruch's Membrane. *Retina Fifth Edition* **1**, 465–481 (2012).
32. McLaughlin, P. J. *et al.* Lack of fibulin-3 causes early aging and herniation, but not macular degeneration in mice. *Hum. Mol. Genet.* https://doi.org/10.1093/hmg/ddm264 (2007).
33. Klenotic, P. A., Munier, F. L., Marmorstein, L. Y. & Anand-Apte, B. Tissue inhibitor of metalloproteinases-3 (TIMP-3) is a binding partner of epithelial growth factor-containing fibulin-like extracellular matrix protein 1 (EFEMP1): Implications for macular degenerations. *J. Biol. Chem.* **279**, 30469–30473 (2004).
34. Wyatt, M. K. *et al.* Interaction of complement factor h and fibulin3 in age-related macular degeneration.*PLoS One.* 2013 Jun 28;8(6):e68088. https://doi.org/10.1371/journal.pone.0068088
35. Padgett, L. C., Lui, G. M., Werb, Z. & Lavail, M. M. Matrix metalloproteinase-2 and tissue inhibitor of metalloproteinase-1 in the retinal pigment epithelium and interphotoreceptor matrix: Vectorial secretion and regulation. *Exp. Eye Res.* **64**, 927–938 (1997).
36. Seddon, J. M. *et al.* Rare variants in CFI, C3 and C9 are associated with high risk of advanced age-related macular degeneration. *Nat. Genet.* **45**, 1366–1373 (2013).

37. Hageman, G. S. *et al.* A common haplotype in the complement regulatory gene factor H (HF1/CFH) predisposes individuals to age-related macular degeneration. *Proc. Natl. Acad. Sci. U. S. A.* **102**, 7227–7232 (2005).
38. Russell, S. R., Mullins, R. F., Schneider, B. L. & Hageman, G. S. Location, substructure, and composition of basal laminar drusen compared with drusen associated with aging and age-related macular degeneration. *Am. J. Ophthalmol.* **129**, 205–214 (2000).
39. Crabb, J. W. *et al.* Drusen proteome analysis: An approach to the etiology of age-related macular degeneration. *Proc. Natl. Acad. Sci. U. S. A.* **99**, 14682–14687 (2002).
40. Maminishkis, A. *et al.* Confluent Monolayers of Cultured Human Fetal Retinal Pigment Epithelium Exhibit Morphology and Physiology of Native Tissue. *Investig. Ophthalmol. Vis. Sci.* **47**, 3612–3624 (2006).
41. Wang, L. *et al.* Abundant lipid and protein components of drusen. PLoS One. 2010 Apr 23;5(4):e10329 https://doi.org/10.1371/journal.pone.0010329
42. DeAngelis, M. M. *et al.* Genetics of age-related macular degeneration (AMD). *Hum. Mol. Genet.* **26**, R45–R50 (2017).
43. Boyer, O. *et al.* Complement Factor H Deficiency and Posttransplantation Glomerulonephritis With Isolated C3 Deposits. *Am. J. Kidney Dis.* https://doi.org/10.1053/j.ajkd.2007.11.032 (2008).
44. Keenan, T. D. L. *et al.* Age-dependent changes in heparan sulfate in human Bruch's membrane: Implications for age-related macular degeneration. *Investig. Ophthalmol. Vis. Sci.* **55**, 5370–5379 (2014).
45. Volland S, Esteve-Rudd J, Hoo J, Yee C, Williams DS. A comparison of some organizational characteristics of the mouse central retina and the human macula. PLoS One. 2015Apr 29;10(4):e0125631. https://doi.org/10.1371/journal.pone.0125631
46. Harman, A. M., Fleming, P. A., Hoskins, R. V. & Moore, S. R. Development and aging of cell topography in the human retinal pigment epithelium. *Investig. Ophthalmol. Vis. Sci.* **38**, 2016–2026 (1997).
47. Del Priore LV, Kuo YH, Tezel TH. Age-related changes in human RPE cell density and apoptosis proportion in situ. Invest Ophthalmol Vis Sci. 2002 Oct;43(10):3312-8.
48. Frick, K. M. Estrogens and age-related memory decline in rodents: What have we learned and where do we go from here?. *Horm. Behav.* **55**, 2–23 (2009).
49. Vingerling, J. R. *et al.* Macular degeneration and early menopause: A Case-control study. *BMJ* **310**, 1570 (1995).
50. Cousins, S. W. *et al.* Female gender, estrogen loss, and sub-RPE deposit formation in aged mice. *Investig. Ophthalmol. Vis. Sci.* **44**, 1221–1229 (2003).
51. Kaarniranta, K. *et al.* Estrogen signalling in the pathogenesis of age-related macular degeneration. *Curr. Eye Res.* **40**, 226–233 (2015).
52. Klein, S. L. & Flanagan, K. L. Sex differences in immune responses. *Nat. Rev. Immunol.* **16**, 626–638 (2016).
53. Ren, W. *et al.* The Complement C3a–C3aR axis promotes development of thoracic aortic dissection via regulation of MMP2 expression. *J. Immunol.* https://doi.org/10.4049/jimmunol.1601386 (2018).
54. Nilsson, B. & Nilsson Ekdahl, K. The tick-over theory revisited: Is C3 a contact-activated protein?. *Immunobiology* **217**, 1106–1110 (2012).
55. Bexborn, F., Andersson, P. O., Chen, H., Nilsson, B. & Ekdahl, K. N. The tick-over theory revisited: Formation and regulation of the soluble alternative complement C3 convertase (C3(H2O)Bb). *Mol. Immunol.* **45**, 2370–2379 (2008).
56. Filho, D. A. G. *et al.* Change in Drusen volume as a novel clinical trial endpoint for the study of complement inhibition in age-related macular degeneration. *Ophthalmic Surg. Lasers Imaging Retin.* **45**, 18–31 (2014).
57. Mattapallil, M. J. *et al.* The Rd8 mutation of the Crb1 gene is present in vendor lines of C57BL/6N mice and embryonic stem cells, and confounds ocular induced mutant phenotypes. *Invest. Ophthalmol. Vis. Sci.* **53**, 2921–2927 (2012).
58. Wetsel, R. A., Fleischer, D. T. & Haviland, D. L. Deficiency of the murine fifth complement component (C5) A 2-base pair gene deletion in a 5'-exon. *J. Biol. Chem.* **265**, 2435–2440 (1990).
59. Sonoda, S. *et al.* A protocol for the culture and differentiation of highly polarized human retinal pigment epithelial cells. *Nat. Protoc.* **4**, 662–673 (2009).

Acknowledgements

This work was supported by the Ocular Genomics Institute. The TEM work was supported in part by a National Eye Institute Core grant (P30EY003790). The authors would like to thank Schepens Eye Research Institute morphology core facility, especially Philip Seifert for performing the TEM, and Ann Tisdale for helpful technical assistance with SM.

Author contributions

D.L.G. performed the in vivo experiments and helped writing the manuscript. E.A.P. supervised the work and edited the manuscript. R.F.G. bred and genotyped the mice, performed all the in vitro experiments and wrote the manuscript.

Competing interests

The authors declare no competing interests.

Additional information

Supplementary Information The online version contains supplementary material available at https://doi.org/10.1038/s41598-021-89978-8.

Correspondence and requests for materials should be addressed to R.F.-G.

Reprints and permissions information is available at www.nature.com/reprints.

Publisher's note Springer Nature remains neutral with regard to jurisdictional claims in published maps and institutional affiliations.